BUTTERWORTH HEINEMANN

Large-eddy simulation of a spatially growing boundary layer over an adiabatic flat plate at low Mach number

F. Ducros, P. Comte, and M. Lesieur
LEGI/Institut de Mécanique de Grenoble, Grenoble, France

A new subgrid-scale model giving nearly zero eddy-viscosity during the laminar and the transition stages of a flow is proposed on the basis of the structure–function model (Métais & Lesieur 1992). With this new model, a large-eddy simulation (LES) of the complete transition of a quasi-incompressible boundary layer is presented. At a computational cost of about 80 CPU hours of Cray 2, statistics and visualizations indicate that the essential features of the transition process and of the turbulent motion are correctly captured.

Keywords: subgrid scale (SGS) modeling; turbulence; boundary layers; large-eddy simulations

Introduction

Four years after the review by Kleiser and Zang (1991), numerical simulation of transition in wall-bounded shear flows is still a challenge. It is often stated that transition involves smaller scales than developed turbulence, which already reaches the limits of the largest super computers currently available. The only direct numerical simulation (DNS) of the complete transition of a spatially growing boundary layer that we know about (Rai and Moin 1993) required 800 hours of Cray Y-MP per run. Nevertheless, a multiblock grid was used in order to minimize unnecessary mesh refinement, the finest meshes lying in the transitional region. On the other hand, since Deardorff (1970), subgrid-scale turbulence models have permitted substantial cost reduction for (large-eddy) simulations of the turbulent regime. Our main objective here is to advocate large-eddy simulations (LES) of the complete transition process down to the turbulent regime, with a model smart enough not to act during the early stages of transition. For reasons of consistency with our investigations of high-Mach number boundary layers (Ducros et al. 1993), we keep the same numerical methods and work at the lowest Mach number for which our code remains effective; i.e., $M_\infty = 0.5$. In the light of Morkovin (1961), this seems to be low enough to permit comparison with incompressible experiments and simulations, at least as a first approximation.

This paper is organized as follows: in the first section, we briefly recall the compressible equations involved in LES and the modeling we adopt. Then, we detail our new subgrid model and provide an a-priori test to prove the insensitivity of this model to such large-scale fluctuations as Tollmien–Schlichting waves. In the third section, we present a LES of the forced transition of a boundary layer at $M_\infty = 0.5$ and $\mathrm{Re}_{\delta_i} = 1000$, with comparisons with incompressible data.

Subgrid modeling

Discretization onto a finite–difference computational grid amounts to the convolution with a discrete low-pass filter (box filter), hereafter denoted $\bar{}$. This operator commutes with time and space derivatives, at least to second-order accuracy. * The filtered compressible Navier–Stokes equations for an ideal gas are thus approximated by the pseudoconservative form

$$\frac{\partial \bar{U}}{\partial t} + \frac{\partial \bar{F}_i}{\partial x_i} = 0, \qquad i \in \{1, 2, 3\} \tag{1}$$

with

$$\bar{U} = {}^T\left(\bar{\rho}, \overline{\rho u_1}, \overline{\rho u_2}, \overline{\rho u_3}, \overline{\rho e}\right) \tag{2}$$

and

$$\overline{\rho e} = \overline{\rho c_v T} + \tfrac{1}{2}\overline{\rho\left(u_1^2 + u_2^2 + u_3^2\right)} \tag{3}$$

The resolved fluxes $\bar{F}_i$ read

$$\bar{F}_i = \begin{pmatrix} \overline{\rho u_i} \\ \overline{\rho u_i u_1} + \bar{p}\delta_{i1} - \overline{\mu S_{i1}} \\ \overline{\rho u_i u_2} + \bar{p}\delta_{i2} - \overline{\mu S_{i2}} \\ \overline{\rho u_i u_3} + \bar{p}\delta_{i3} - \overline{\mu S_{i3}} \\ \overline{(\rho e + p)u_i} - \overline{\mu S_{ij} u_j} - k\overline{\dfrac{\partial T}{\partial x_i}} \end{pmatrix} \tag{4}$$

Address reprint requests to Dr. P. Comte, LEGI/Institut de Mécanique de Grenoble, B.P. 53X, F38041 Grenoble Cedex, France.

Received 19 January 1995; accepted 6 December 1995

* Here, the mesh length and width are constant. Commutation with $\partial/\partial x_1$ and $\partial/\partial x_3$ are, therefore, exact. Commutation with $\partial/\partial x_2$ and $\partial/\partial t$ are only second-order accurate, because of grid stretching in the direction normal to the wall and the variable time step which ensures constant CFL.

Int. J. Heat and Fluid Flow 16: 341–348, 1995

655 Avenue of the Americas, New York, NY 10010

0142-727X/95/$10.00
SSDI 0142-727X(95)00049-V

with

$$S_{ij} = \left[\frac{\partial u_j}{\partial x_i} + \frac{\partial u_i}{\partial x_j} - \frac{2}{3}(\nabla \cdot \mathbf{u})\delta_{ij} \right] \tag{5}$$

and the filtered equation of state $\bar{p} = R\overline{\rho T}$. Closure of the system requires that the fluxes $\overline{F_i}$ are computable out of $\overline{U}$; that is, $\bar{\rho}$ and the Favre-filtered components $\tilde{u}_i = \overline{\rho u_i}/\bar{\rho}$ and $\tilde{e} = \overline{\rho e}/\bar{\rho}$. We, therefore, introduce a subgrid-stress tensor $\mathscr{T}$ defined by

$$\mathscr{T}_{ij} = -\overline{\rho u_i u_j} + \bar{\rho}\tilde{u}_i\tilde{u}_j \tag{6}$$

and close its deviatoric part with the aid of an eddy-viscosity coefficient $\nu_t(\mathbf{x}, t)$:

$$-\overline{\rho u_i u_j} \simeq -\bar{\rho}\tilde{u}_i\tilde{u}_j + \bar{\rho}\nu_t\widetilde{S_{ij}} \qquad \text{for} \qquad i \neq j \tag{7}$$

As in the incompressible LES formalism, we introduce a macro-pressure

$$\varpi = \bar{p} - \tfrac{1}{3}\mathscr{T}_{ll} \tag{8}$$

The "macro temperature"

$$\vartheta = \tilde{T} - \frac{1}{2c_v\bar{\rho}}\mathscr{T}_{ll} \tag{9}$$

is computable thanks to Equation 3 rewritten as:

$$\overline{\rho e} = \bar{\rho}c_v\vartheta + \tfrac{1}{2}\bar{\rho}\left(\widetilde{u_1^2} + \widetilde{u_2^2} + \widetilde{u_3^2}\right) \tag{10}$$

The filtered equation of state then reads

$$\varpi = \bar{\rho}R\vartheta + \frac{3\gamma - 5}{6}\mathscr{T}_{ll} \simeq \bar{\rho}R\vartheta \tag{11}$$

with exact equality in the case of helium or argon.

The energy equation is closed in an even cruder fashion, assuming

$$-\overline{(\rho e + p)u_i} + \overline{\mu S_{ij}u_j} + k\overline{\frac{\partial T}{\partial x_i}} \simeq$$

$$-(\overline{\rho e} + \varpi)\tilde{u}_i + \mu\widetilde{S_{ij}}\tilde{u}_j + \left[\frac{c_p}{\mathrm{Pr}}\mu + \frac{c_p}{\mathrm{Pr}_t}\bar{\rho}\nu_t\right]\frac{\partial\vartheta}{\partial x_i} \tag{12}$$

with $\mathrm{Pr}_t = \mathrm{Pr}_t = 1$. The resolved fluxes are thus modeled as:

$$\overline{F_i} \simeq \begin{pmatrix} \bar{\rho}\widetilde{u_i} \\ \bar{\rho}\widetilde{u_i}\widetilde{u_1} + \varpi\delta_{i1} - [\mu + \bar{\rho}\nu_t]\widetilde{S_{i1}} \\ \bar{\rho}\widetilde{u_i}\widetilde{u_2} + \varpi\delta_{i2} - [\mu + \bar{\rho}\nu_t]\widetilde{S_{i2}} \\ \bar{\rho}\widetilde{u_i}\widetilde{u_3} + \varpi\delta_{i3} - [\mu + \bar{\rho}\nu_t]\widetilde{S_{i3}} \\ (\bar{\rho}\tilde{e} + \varpi)\widetilde{u_i} - \mu\widetilde{S_{ij}}\widetilde{u_j} - \left[\frac{c_p}{\mathrm{Pr}}\mu + \frac{c_p}{\mathrm{Pr}_t}\bar{\rho}\nu_t\right]\frac{\partial\vartheta}{\partial x_i} \end{pmatrix} \tag{13}$$

Filtered structure-function model

Normand and Lesieur (1992) simulated transition of a boundary layer at Mach 5 thanks to the structure–function (SF) model proposed by Métais and Lesieur (1992) without any compressibility correction. This model reads

$$\nu_t^{\mathrm{SF}}(\mathbf{x}, t) = 0.105C_K^{-3/2}\Delta\left[\widetilde{F_2}(\mathbf{x}, \Delta, t)\right]^{1/2} \tag{14}$$

in which $C_K \approx 1.4$ denotes Kolmogorov's constant. $\widetilde{F_2}(\mathbf{x}, \Delta, t)$ is the second-order structure function of the resolved velocity field $\tilde{\mathbf{u}}$ at scale Δ

$$\widetilde{F_2}(\mathbf{x}, \Delta, t) = \langle \| \tilde{\mathbf{u}}(\mathbf{x} + \mathbf{r}, t) - \tilde{\mathbf{u}}(\mathbf{x}, t) \|^2 \rangle_{\|\mathbf{r}\| = \Delta} \tag{15}$$

evaluated over the four closest neighbors of point $\mathbf{x}$ on a plane parallel to the wall. This stencil is too local to be insensitive to growing eigenmodes during transition, although they were quite well resolved. The dominant instability at Mach 5 being inviscid in nature (Mack's second mode), this did not prevent transition as it would do at our Mach number 0.5.

To remedy this without changing the philosophy of the structure–function model (consistency with spectral models derived from EDQNM considerations in isotropic turbulence following Kolmogorov spectra) we propose to apply a high-pass filter onto $\mathbf{u}$ before computing its structure function. An exact Laplacian filter iterated n times would, in the Fourier space, multiply the energy spectrum $E(k)$ by k^{4^n}. This is simple enough to be included in the derivation of the SF model in Métais and Lesieur

Notation

$C_f(x_1)$ and $H_{12}(x_1)$	friction coefficient and shape factor
$E(k_C)$	kinetic energy isotropic spectrum at the cut-off wave number $k_C = \pi/\Delta$
$\tilde{F}_2(\mathbf{x}, \Delta, t)$ and $\tilde{F}_{2HP^n}(\mathbf{x}, \Delta, t)$	second-order structure functions of $\tilde{u}$ and $HP^n(\tilde{\mathbf{u}})$
$HP^n(\tilde{\mathbf{u}})$	resolved velocity field after its filtering by a discrete Laplacian iterated n times
$L_{x_1} = 812\ \delta_i$, $L_{x_2}L_{x_3} = 20\ \delta_i$	dimensions of the domain
$M_\infty = U_\infty/a_\infty = 0.5$	external Mach number
$\mathrm{Re}\delta_i = \rho_\infty U_\infty\delta_i/\mu_\infty = 1{,}000$	inlet Reynolds number
U_∞ $T_\infty = 273K$, ρ_∞, a_∞, and μ_∞:	stream-wise velocity, temperature, density, speed of sound, and dynamic viscosity at $x_2 \to \infty$
δ_1	displacement thickness, $\delta_i = \delta_1(x = 0)$
Re_x	stream-wise Reynolds number
$\tilde{\mathbf{u}}(\mathbf{x}, t)$	resolved velocity field (Favre filtered)
u'_1, u'_2, u'_3	components of the rms fluctuations of $\tilde{\mathbf{u}}$ with respect to its time average $\langle\tilde{\mathbf{u}}\rangle(\mathbf{x})$
x_1, x_2, x_3	stream-wise, normal-to-the-wall, and span-wise coordinates of point x
Greek	
$\Delta x_2(x_2)$	mesh size in the direction normal to the wall; Δx_1 and Δx_3 are constant; $\Delta(x_2) = (\Delta x_1\Delta x_2\Delta x_3)^{1/3}$
$\nu_t(\mathbf{x}, t)$, $\kappa_t(\mathbf{x}, t)$	local eddy-viscosity and eddy-diffusivity coefficients
$\rho(\mathbf{x}, t)$, $p(\mathbf{x}, t)$, $T(\mathbf{x}, t)$, $\mu(T)$	density, pressure, temperature, and viscosity (given by Sutherland's law)

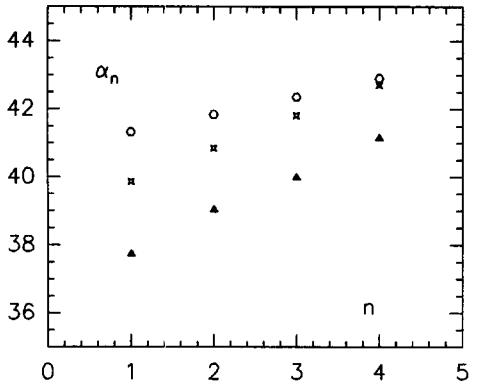

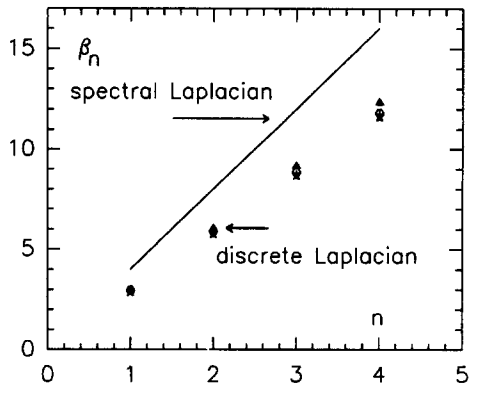

Figure 1 Values of α_n (left) and β_n (right) as a function of n for different realizations of $\tilde{\mathbf{u}}$: 3-D white noise (triangles); initial condition (crosses); and self-similar stage (circles) in a DNS of isotropic turbulence at resolution 32^3; a spectral Laplacian filter would give $\alpha_n = 1$ and $\beta_n = 4n$

(1992), yielding a formulation analogous to Equation (14), up to the constant's value. Approximated by second-order centered finite differences

$$HP^n(\bar{\mathbf{u}}(\mathbf{x}, t)) = \Big[\underbrace{HP^1 \circ \ldots \circ HR^1}_{n \text{ times}}\Big]\bar{\mathbf{u}}(\mathbf{x}, t) \tag{16}$$

with

$$HP^1[\tilde{\mathbf{u}}(\mathbf{x})] = \sum_{i=2,3} [\tilde{\mathbf{u}}(\mathbf{x} - \Delta\mathbf{x}_i) - 2\tilde{\mathbf{u}}(\mathbf{x}) + \tilde{\mathbf{u}}(\mathbf{x} + \Delta\mathbf{x}_i)], \tag{17}$$

iterated Laplacian filters satisfy approximately laws of the form

$$\frac{\tilde{E}_{HP^n}(k)}{\tilde{E}(k)} = \alpha_n^n \left(\frac{k}{k_C}\right)^{\beta_n}. \tag{18}$$

Figure 1 shows that $\alpha_n = 40$, and $\beta_n = 3n$ is an acceptable fit for a representative set of flow fields, at least up to $n = 4$. These values do not seem to depend much on resolution. They yield

$$\nu_t^{FSF_n}(\mathbf{x}, t) = \gamma_n C_K^{-3/2} \Delta \left[\widetilde{F}_{2HP^n}(\mathbf{x}, \Delta, t)\right]^{1/2} \tag{19}$$

with

n	0	1	2	**3**	4
γ_n	0.105	0.033	0.0071	**0.0014**	$2.6\ 10^{-4}$

$\widetilde{F}_{2HP^n}(\mathbf{x}, \Delta, t)$ being the structure function of the filtered resolved field $HP^n(\tilde{\mathbf{u}})$, computed as in Equation 15.

Different tests (a priori and a posteriori) with different numerical methods show that the least dissipative filtered structure–function model which works corresponds to $n = 3$. The reader is referred to Comte et al. (1994) for comparisons between the FSF_3 model and four other models in the case of incompressible mixing layers simulated at zero molecular viscosity with a spectral code (resolution 64^3): the FSF_3 model gives results very similar to the spectral model and the selective structure-function model proposed by David (1995). See also Lesieur and Métais (1995) for a review, and Silvestrini et al. (1995) in which spatially growing simulations of an incompressible mixing layer are performed with the FSF_3 model.

Figure 2 suggests that the FSF_3 model is consistent with the original SF model in the case of incompressible isotropic turbulence, treated with (nondissipative) pseudospectral methods. This has recently been confirmed at resolution 64^3.

Superiority of FSF_3 for transitional flows is evident when looking at its asymptotic behavior in the case of a discrete longitudinal sine wave $\tilde{\mathbf{u}}_{i,j,k} = U\cos(\omega i + \phi)$ of pulsation $\omega = k\Delta = \pi k/k_c$ and phase ϕ, in the long-wave limit $\omega \to 0$. For this signal, the SF model yields

$$\widetilde{F}_2(\mathbf{x}, \Delta, t) = U^2\{[2\sin^2\phi]\omega^2 + [4i\cos\phi\sin\phi]\omega^3 + \left[\left(\tfrac{1}{2}\cos^2\phi - \tfrac{2}{3}\sin^2\phi\right) + 2i^2(\cos^2\phi - \sin^2\phi)\right]\omega^4 + \mathcal{O}(\omega^5)\}, \tag{20}$$

i.e., scales in general on ω^2. The eddy-viscosity given by the SF model then scales on ω. On the other hand,

$$\widetilde{F}_{2HP^n}(\mathbf{x}, \Delta, t) = [2(\cos\omega - 1)]^n \widetilde{F}_2(\mathbf{x}, \Delta, t) \tag{21}$$

which gives a scaling in ω^{2n+1} for the FSF_n model.

Spatially developing boundary layer

System 1, 2, 10, 11, 13, 19 is solved by means of the code developed by Normand and Lesieur (1992). This code is based on an explicit McCormack-type scheme, which is fourth-order accurate in space (and second-order accurate in time, see Gottlieb and Turkel 1976). In the case of a temporal boundary layer at Mach 4.5, the growth rates of Mack's second mode and its most

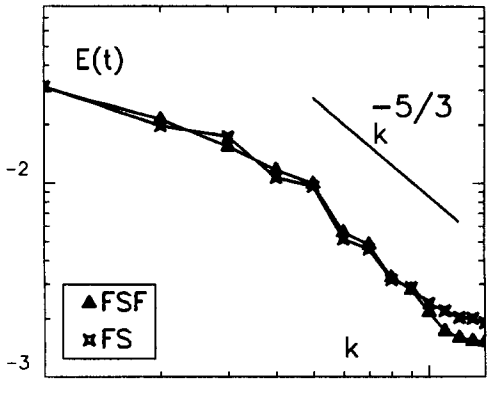

Figure 2 Kinetic energy spectra in freely decaying turbulence simulated a zero molecular viscosity with the FSF_3 and SF models (resolution 32^3)

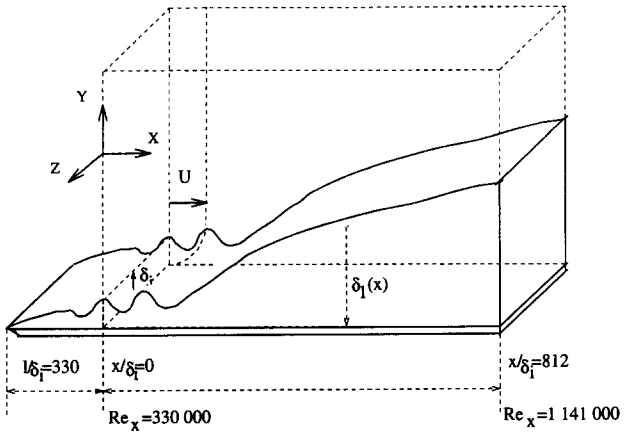

Figure 3 Localization of our calculation box with respect to a virtual leading edge

amplified oblique subharmonics were predicted correctly (Ducros et al. 1993), which can be considered as a valuable validation.

For the spatially growing simulation presented here, we consider a domain as sketched in Figure 3. Adherence and adiabaticity are prescribed at the wall: ($\tilde{\mathbf{u}} = \mathbf{0}$ and $\partial\vartheta/\partial x_2 = 0$ for $x_2 = 0$). Nonreflective conditions (Thompson 1987) are used for all other boundaries, except in the spanwise direction x_3, where periodicity is enforced. At the inlet $x_1 = 0$, we impose, on the incoming characteristics, a laminar profile $U_{i_{lam}}(x_2)$ solution to the similarity equations at $M_\infty = 0.5$, with small-amplitude perturbations renewed every time step:

$$\tilde{u}_i(0, x_2, x_3, t) = U_{i_{lam}}(x_2)$$
$$+5\ 10^{-3}\varepsilon_{2D}\hat{u}_i(x_2)\ \sin[\omega t + \phi(x_2)]$$
$$+8\ 10^{-3}\varepsilon_{3D}x_2^2 e^{-x_2}\Upsilon(x_2, x_3, t)U_\infty \qquad (22)$$

$\hat{u}_i(x_2)$ and $\phi(x_2)$ are the amplitude (normalized by U_∞) and phase profiles of the most amplified mode [two-dimensional (2-D) Tollmien–Schlichting waves] at $M_\infty = 0.5$ and $\mathrm{Re}_\infty = 1000$, based on the displacement thickness δ_i of $U_{i_{lam}}(x_2)$. Υ is a random function (white noise) giving values between 0 and 1. Analogous forcing is applied to the pressure.

The computational domain is sketched below. It extends from $x = 0$ to 812 δ_i. Its other dimensions are $L_{x_2} = L_{x_3} = 20\ \delta_i$, which is rather small. We have carefully checked the behavior of the upper boundary condition in this configuration (Ducros 1995). The resolution is $N_{x_1} = 650$, $N_{x_2} = 32$, and $N_{x_3} = 20$. The meshes

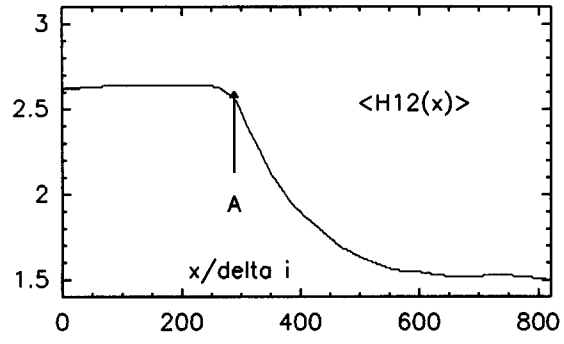

Figure 4 Spatial distribution of the shape factor $\langle H_{12}(x)\rangle$ (A is located at $x \approx 280\delta_i$)

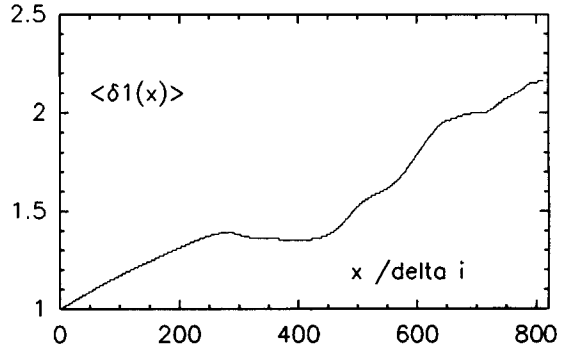

Figure 5 Streamwise distribution of the displacement thickness $\langle \delta_1(x)\rangle$

are uniform in the stream-wise and span-wise directions. Stretching is applied in the direction normal to the wall, through

$$x_2(j) = L_{x_2}\frac{0.3\eta}{1.3 - \eta}, \qquad \eta = \frac{j-1}{N_{x_2} - 1} \qquad (23)$$

Calculations and statistical results

At $t = 0$, we impose a 2-D flow resulting from a 2-D calculation in the whole box. We perform the 3-D 2-D simulation up to a time corresponding to 2.35 advections of the domain at the speed of the T-S waves ($0.35U_\infty$), which requires about 80 hours of CPU time on a Cray 2. Visualizations and time-averaged statistics are performed during the last $240\delta_i/U_\infty$ of the simulation, for which the influence of the initial conditions should not be significant.

The time-averaged displacement thickness $\langle \delta_1(x)\rangle$ and shape factor $\langle H_{12}(x)\rangle$ are plotted in Figures 4 and 5.

We have checked that $\langle \delta_1(0)\rangle = \delta_i$, and that $\langle \delta_1(x)\rangle$ grows $\propto x^{1/2}$ during the laminar stage and approximately $\propto x^{0.76}$ between 500 and 812 δ_i (*vs.* $x^{0.83}$ in Cousteix 1989). The shape factor is 2.8 for the laminar regime and 1.6 for the turbulent stage, to be compared with the values 2.6 and 1.5 found in Cousteix (1989), in the incompressible case. Transition occurs at $x = 280\ \delta_i$; i.e., $\mathrm{Re}_x = 600\ 10^3$ (point A in Figure 4).

The friction coefficient is plotted in Figure 6, together with the theoretical laws $C_f = 0.664\ \mathrm{Re}_x^{-1/2}$ and $C_f = 0.0368\ \mathrm{Re}_x^{-1/6}$ for incompressible Blasius and turbulent profiles, respectively.

The former law is well verified, which suggests that the model behaves correctly up to transition. Unfortunately, the usual over-

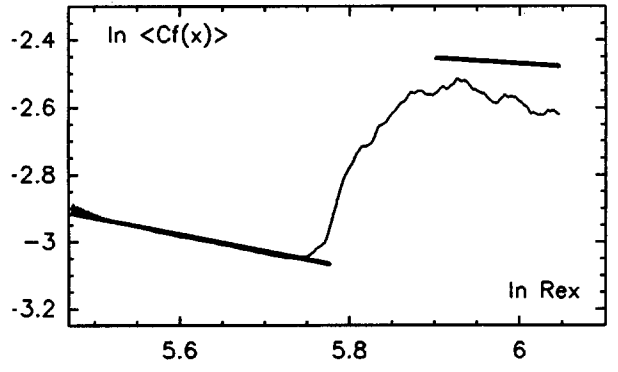

Figure 6 Spatial distribution of the friction coefficient $\langle C_f\rangle(x_1)$, averaged over time and the spanwise direction x_3

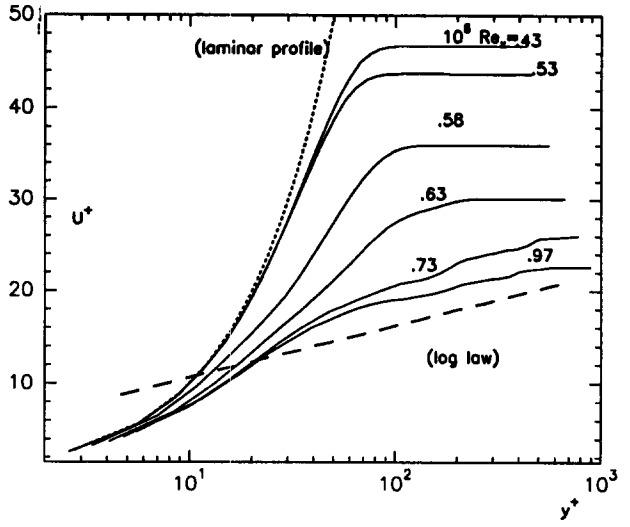

Figure 7 Time- and spanwise-averaged stream-wise velocity profiles, in wall units, for several streamwise positions

shoot of C_f is not visible, and C_f decays too fast later. We believe that this is mainly due to the model, which seems to be too dissipative in the turbulent regime.

Figure 7 shows the spatial evolution of the mean stream-wise velocity profile in wall units, in function of Re_x. The last profile is compared with the empirical law $U^+ = 2.44 \ln y^+ + 5.$, which confirms that the friction velocity is too low: we measured $u_\tau/U_\infty \approx 0.038$ for $x \approx 550\ \delta_i$, to be compared with the value 0.046 obtained by Spalart (1988) in DNS at the same Reynolds number.

Figure 8 shows profiles of rms velocity fluctuations normalized by u_τ, recorded at $\mathrm{Re}_x \approx 10^6$. The horizontal coordinate is the distance to the wall y_2, divided by the local boundary-layer thickness $\delta_{99\%}$. Agreement with respect to the DNS of Spalart (1988) is acceptable for u'_1. As mentioned by Antonia et al. (1992), higher resolution is needed in order to get u'_2 and u'_3 correct.

The Reynolds stress profiles are nearly constant throughout the layer (except near the wall, see Figure 9 where experimental results of Sabot and Comte-Bellot, 1976 are plotted).

Visualizations

In all the figures to come, the boundary layer flows from left to right, and the domain has been duplicated in the span-wise direction in order to make the flow topology more evident. Figure 10 shows contours of u'_1 on the plane $x_2 = .27\ \delta_i$ (i.e., $x_2^+ = 11.8$). Up to 280 δ_i, the span-wise stripes correspond to TS waves. Λ structures are visible from 280 to 350 δ_i. Further downstream, stream-wise streaks are visible. Their span-wise spacing is $\approx$ 130 wall units, the commonly accepted value being 100.

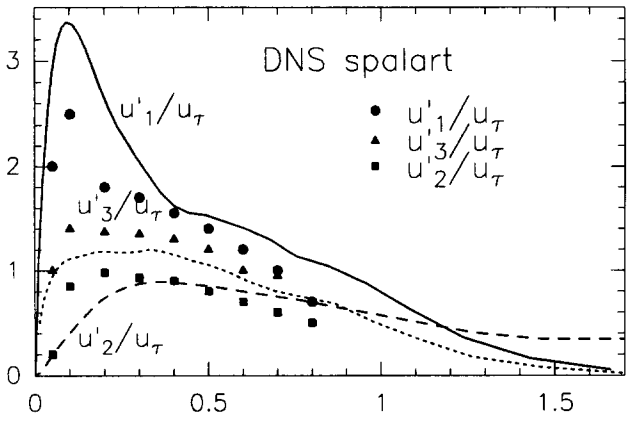

Figure 8 Time- and spanwise-averaged profiles of rms velocity fluctuation profiles compared to Spalart's (1988)

From the zoom shots, Figures 11 and 12, the period of the TS waves can be estimated to be about 21 δ_i. The transition point A at $x_1 = 280\ \delta_i$, beyond which the shape factor drops, corresponds to the beginning of the three-dimensionalization of these waves. The first Λ structure forms at about 300 δ_i, in the staggered arrangement. This can be seen as evidence of a H-type mode (Herbert 1988). More precisely, in this region, the turbulent kinetic energy grows exponentially with x_1 at a rate $\gamma_r = 1.95\ 10^{-2}\ \delta_i^{-1}$ close to the value $2.2\ 10^{-2}$ found by Herbert for the most amplified oblique subharmonic mode of secondary instability. The domain is, nevertheless, too narrow to respect the span-wise period of this mode ($\lambda_z \approx 1.5\lambda_x = 31.5\ \delta_i$, against $L_z = 20\ \delta_i$). Note also in Figures 11 and 12 the small scales, which form at about $x_1 = 400\ \delta_i$.

The low-pressure isosurfaces (Figure 11) are well correlated spatially with the head of the Λ-shaped structures materialized by the isosurfaces of stream-wise vorticity: high-vorticity magnitude can be found in the same place. Vertical pumping of low fluid

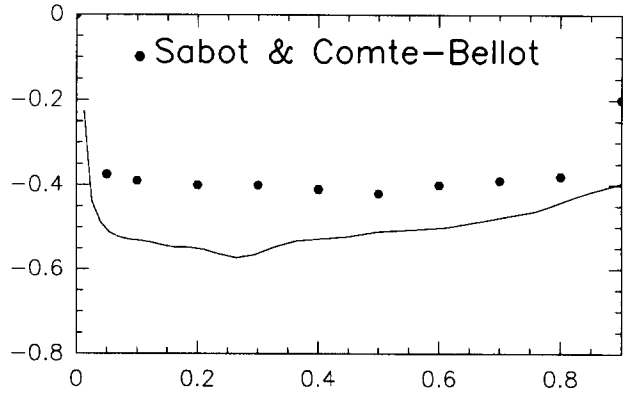

Figure 9 Reynolds stress profiles $(u'_1u'_2)/(u_{1_{\mathrm{rms}}}u_{2_{\mathrm{rms}}})$ together with the experimental results of Sabot and Comte-Bellot (1976) reported in Moin and Kim (1981)

Figure 10 Horizontal slice at $x_2 = 0.27\delta_i$ ($x_2^+ \approx 11.8$) of the stream-wise velocity fluctuations u'_1; the whole domain is shown

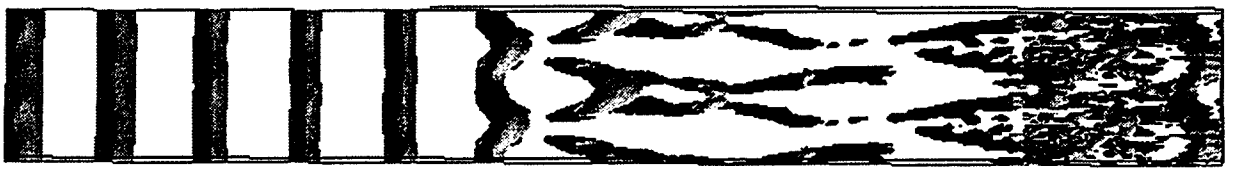

Figure 11 Zoom on the transitional zone between 149 and 454 δ_i, showing, from the top, isosurfaces $|\omega_{x_1}| = 0.1U_\infty/\delta_i$ (dark gray) and $p = 0.992P_\infty$ (light gray)

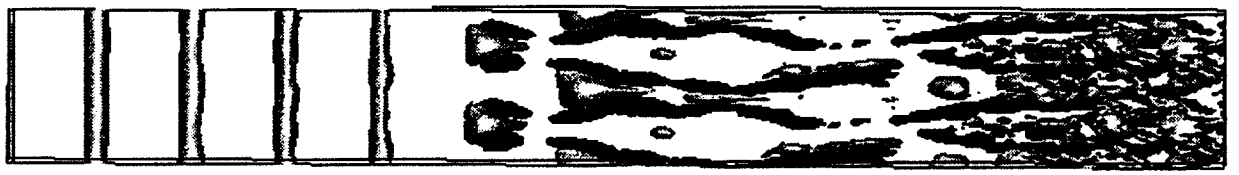

Figure 12 Same view as before, with isosurface $u_2 = 0.007U_\infty$ instead of the low-pressure isosurface

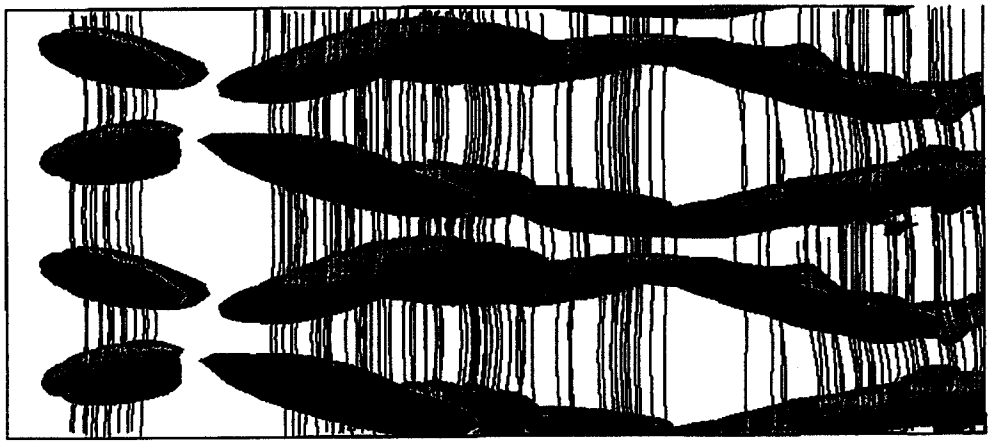

Figure 13 Close-up between 260 and 375 δ_i showing, still from the top, isosurfaces $\omega_{x_1} = \pm 0.15U_\infty/\delta_i$ (light gray) and $\omega_{x_1} = 0.15U_\infty/\delta_i$ (light gray), plus the most 3-D vortex lines

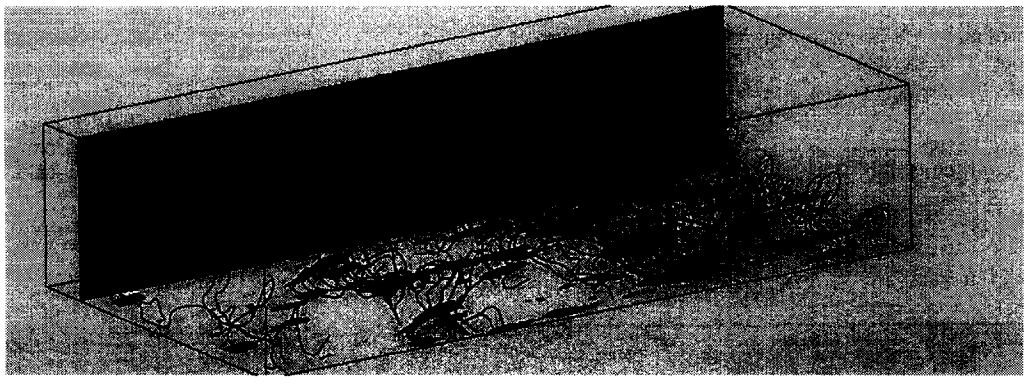

Figure 14 Perspective view of the transitional zone between 474 and 553 δ_i showing, again, isosurfaces $\omega_x = \pm 0.15U_\infty/\delta_i$ (light and dark gray, respectively), the most 3-D vortex lines and a vertical slice with ω_{x_3} contours

Figure 15 Same as Figure 12, without the iso-$|\omega_{x_1}|$ surface, replaced by isosurface $\nu_t = 0.33\mu_\infty/\rho_\infty$ given by the FSF_3 model, (dark gray)

Figure 16 Same as Figure 15, but with ν_t computed a priori with the original SF model, from the same velocity field

takes places between the legs of these Λ structures, as shown in Figure 12: notice white patterns of positive value in between the dark Λ-shaped structures. However, the level of three-dimensionality is still very low, as shown by the very small deformation of the vortex lines in Figure 13. This is obviously no longer the case further downstream: Figure 14 shows isosurfaces of ω_{x_1} stretched at the wall, in the stream-wise direction. Ejections are visible from the span-wise vorticity contours on the vertical slice in Figure 14. Maximum values of ω_{x_3} are found immediately downstream of the tip of the hairpin vortices materialized by the vortex lines in Figure 14. This confirms the classical interpretation of transition to turbulence in terms of break-down of local mixing layers downstream of the hairpin vortices.

Spatial distribution of eddy-viscosities

Figure 15 shows an isosurface of eddy-viscosity, together with an isosurface of u_2'. The latter is there to show where the FSF_3 model acts most. This surface is repeated in Figure 16, which also shows an isosurface of the eddy-viscosity that would give the original SF model from the same resolved velocity field. The threshold is, of course, the same as in Figure 15. In the turbulent part of the domain ($x \leqslant 400\ \delta_i$), both models give about the same values of ν_t. This suggests that the constant of the FSF_3 model is correct. In the transitional region, the SF model is obviously more dissipative. Moreover, restarting the simulation with the SF model instead of the FSF_3 model rapidly yields complete relaminarization of the flow.

Conclusions

A low-resolution simulation of the transition of a quasi-incompressible boundary layer is presented. Thanks to the filtered structure function model proposed in this paper, all stages of transition are qualitatively reproduced, although there is only one mesh line in the viscous sublayer (first point at $x_2^+ \approx 3$). This would not have been possible with such a low level of upstream forcing, either with Smagorinsky's model or the SF model, at least at comparable numerical cost. Statistics, nevertheless, show excessive dissipation in the late-transition and turbulent regimes, suggesting that the new model is still overdissipative (see Lamballais et al. 1995, or Comte et al. 1995 for improvement in this respect). The fact that the domain is too narrow to permit the development of a complete spanwise period of H-mode might also contribute to this tendency. Finally, no visible compressibility effects have been noticed at Mach 0.5.

Acknowledgments

This work was supported by DRET and the CNRS (IDRIS). The help of P. Begou for computing and graphical assistance is particularly acknowledged. We also thank R. Gathmann, E. Lamballais, O. Métais, and S. Prestemon for useful discussions. The final version of this paper has greatly benefited from the referees' comments.

References

Antonia, A., Teitel, M., Kim, J. and Browne, L. W. B. 1992. Low Reynolds numbers effects in a fully developed turbulent channel flow. *J. Fluid Mech.*, **236**, 579–605

Comte, P., David, E., Ducros, F., Lamballais, E. Lesieur, M., Métais, O. and Silvestrini, J. H. 1995. *Workshop on Small-scale structures in 3D hydro- and magnetohydrodynamic turbulence*, to appear in *Lecture notes in Physics*, Springer, Berlin

Comte, P., Ducros, F., Silvestrini, J., David, E., Lamballais, E., Métais, O. and Lesieur, M. 1994. Simulation des grandes échelles d'écoulements transitionnels. 74th *AGARD Fluid Dynamics Symposium on Application of Direct and Large-Eddy Simulation to Transition and Turbulence*, Chania

Cousteix, J. 1989. Turbulence et Couche Limite. Cepadues-Editions

David, E. 1993. Modélisation des ecoulements compressibles et hypersoniques: Une approche instationnaire. Ph.D. thesis, National Polytechnic Institute, Grenoble, France

Deardorff, J. W. 1970. A numerical study of three-dimensional turbulent channel flow at large Reynolds number. *J. Fluid Mech.*, **41**, 453–480

Ducros, F., Comte, P. and Lesieur, M. 1993. Ropes and lambda vortices in direct and large-eddy simulations of a high-Mach number boundary layer over a flat plate. In *Selected Proceedings of Turbulent Shear Flows 9*, Springer-Verlag, Berlin

Ducros F. 1995. Simulations numériques directes et des grandes échelles de couches limites compressibles. Ph.D. thesis, National Polytechnic Institute, Grenoble, France

Gottlieb, D. and Turkel, E. 1976. Dissipative two-four methods for time-dependent problems. *Math. Comp.*, **30**, 703–723

Herbert, T. 1988. Secondary instability of boundary layers. *Ann. Rev. Fluid Mech.*, **20**, 487–526

Kleiser, L. and Zang, T. A. 1991. Numerical simulation of transition in wall-bounded shear flows. *Annu. Rev. Fluid Mech.*, **23**, 495–537

Lamballais, E., Lesieur, M. and Métais, O. 1995. Large-eddy simulations of a rotating turbulent channel using a spectral eddy-viscosity, in preparation for submission to *Phys. Fluids.*

Lesieur, M. and Métais, O. 1995. New trends in large-eddy simulations of turbulence. *Annu. Rev. Fluid Mech.*, **28** (in press)

Métais, O. and Lesieur, M. 1992. Spectral large-eddy simulation of isotropic and stably stratified turbulence, *J. Fluid Mech.*, **239**, 157–194

Moin, P. and Kim, J. 1981 Numerical investigation of turbulent channel flow. *J. Fluid Mech.*, **118**, 341–377

Morkovin M. V. 1961. Effects of compressibility on turbulent flows. In *Mécanique de la Turbulence*, colloque CNRS n. 108, ed. C. N. R. S., 367–380

Normand, X. and Lesieur, M. 1992. Direct and large-eddy simulation of transition in the compressible boundary layer. *Theor. Comp. Fluid Dyn.*, **3**, 231

Rai, M. M. and Moin, P. 1993. Direct numerical simulation of transition and turbulence in a spatially evolving boundary layer. *J. Comp. Phys.*, **109**, 169–192

Sabot, J. and Comte-Bellot, G. 1976. Intermittency of coherent structure in the core region of fully developed turbulent pipe flow. *J. Fluid Mech.*, **74**, 767–796

Silvestrini, J. H., Comte, P. and Lesieur, M. 1995. DNS and LES of incompressible mixing layers developing spatially. to appear in *Proc. 10th. Symposium on Turbulent Shear Flows*

Sfalart, P. R. 1988. Direct simulation of a turbulent boundary layer up to $R\theta = 1{,}410$. *J. Fluid Mech.*, **187**, 61–98

Thompson K. W. 1987. Time-dependent boundary conditions for hyperbolic systems. *J. Comp. Phys.*, **68**, 506–517